From 5G Single-Cell Signals to Pervasive Smartphone Positioning: A Real-World Study

Stavros Eleftherakis*
New York University Abu Dhabi,
United Arab Emirates
se2937@nyu.edu

Domenico Giustiniano
IMDEA Networks, Spain
domenico.giustiniano@networks.imdea.org

Yuxin Zhao
Ericsson AB, Sweden
yuxin.zhao@ericsson.com

Xiaolin Jiang
Ericsson AB, Sweden
xiaolin.jiang@njupt.edu.cn

Gustav Lindmark
Ericsson AB, Sweden
gustav.lindmark@ericsson.com

Fredrik Gunnarsson
Ericsson Research, Sweden
fredrik.gunnarsson@ericsson.com

***Abstract*—Accurate and reliable positioning is a cornerstone of pervasive computing. However, GNSS is not always available for pervasive services while cellular-network-based alternatives have proven unsuccessful, due to coarse position accuracy or complex network setup. In this work, we investigate 5G single-cell positioning by leveraging Timing Advance and Angle of Arrival measurements, two key indicators already used in 5G NR for communication. Our approach does not require tight network synchronization among base stations, unlike other 5G positioning techniques. We present the first real-world study of single-cell positioning in a 5G network with a commercial gNB and an off-the-shelf smartphone moving up to 461 meters away from the gNB across four urban trajectories. Our analysis reveals two key challenges: coarse angular and timing resolution, and severe angle and range errors under Non-Line-of-Sight (NLOS) conditions. To overcome these challenges, we present a framework that (i) synthesizes higher-resolution Angle-of-Arrival estimates from real 5G beam patterns, (ii) classifies LOS/NLOS conditions with a Convolutional Neural Network trained on beam signal-strength heatmaps, and (iii) refines angle and ranging using multipath-aware corrections. Our system reduces the median positioning error from $86.8\,m$ to $16.5\,m$ with a single gNB, without the aid of external sensors.**

***Index Terms*—5G, Angle of Arrival, Timing Advance, Smartphone Positioning**

I. Introduction

Accurate and reliable positioning plays a fundamental role in pervasive computing. However, alternative infrastructures to Global Navigation Satellite System (GNSS) are needed. These should already be widely deployed, accessible with commodity devices, and able to operate in GNSS-challenged conditions with poor positioning accuracy or low number of visible satellites [1]. Fifth Generation (5G) mobile networks offer such an opportunity. Alongside high data rates and low latency, 5G New Radio (NR) introduces standardized positioning methods.

Among these, NR Enhanced Cell ID (E-CID) is particularly promising: it relies on Timing Advance (TA) and Angle of Arrival (AoA) measurements, two key indicators already widely used in 5G NR communications. An illustration of the concept is shown in Fig. 1. This approach enables positioning from a single base station (gNB), providing an infrastructure-light solution for pervasive positioning. For instance, a private network operator could deploy a single gNB to offer new services to its users. Yet despite its standardization, the real-world performance of NR E-CID remains largely unknown, particularly when applied to commodity smartphones in operational networks.

* Stavros Eleftherakis carried out this work during his PhD studies at Universidad Carlos III de Madrid (UC3M) and IMDEA Networks Institute.

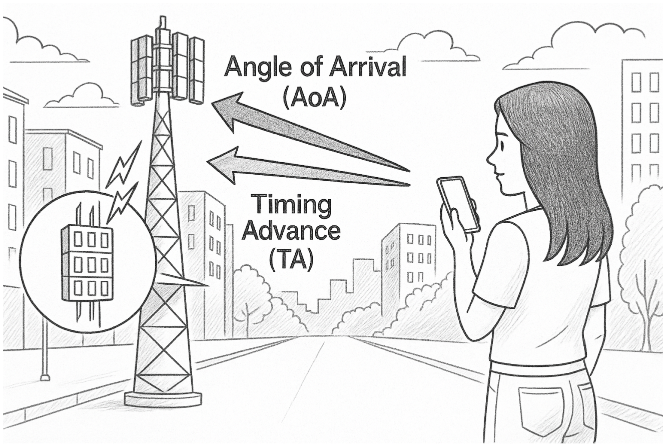

Fig. 1: Illustration of the concept studied: 5G single-cell signals widely available for communication are used for pervasive smartphone positioning.

In this work, we bridge this gap by conducting the first real-world study of NR E-CID positioning with a commercial 5G gNB and an off-the-shelf smartphone in an urban testbed representative of live deployments set up in a major European city. Our analysis identifies two core challenges. The first challenge is that the AoA estimation used for positioning the mobile device is based on the large antenna arrays in 5G MIMO systems —commonly referred to as *Massive MIMO*— as the one deployed in our test network. 5G MIMO features transmission and reception of beams in a given direction within a cell, providing narrower angular coverage than cell-wide communication and prior sector-wide communication.

However, we experimentally observe that the AoA resolution for NR E-CID positioning is limited to the number of beams. Besides, these beams have fixed directions in 5G MIMO systems, as they are primarily used for communication purposes such that multiple users can send data at the same time. We address this challenge by proposing a novel solution to increase the resolution of AoA measurements leveraging the individual angular beam shapes in experimental planar antenna arrays. Commercial 5G gNBs almost consistently use planar Massive MIMO arrays for 3D beamforming and alignment with the 3rd Generation Partnership Project (3GPP) models. Since our approach relies on the geometry of such planar arrays, it generalizes across vendors.

The second challenge is that NR E-CID positioning relies on estimating the distance using 5G TA [2]. We experimentally find that 5G TA used in single-cell 5G positioning largely suffers from limited resolution and Non-Line-of-Sight (NLOS) conditions. Currently, there is no solution to monitor the integrity of ranging estimates acquired from 5G TA measurements. The large antenna arrays in the commercial 5G MIMO systems enable us to address this problem. We then take advantage of the availability of receiver signal strength measurements per beam using an antenna array of 64 logical antenna ports in our 5G test network. We find that these measurements capture Line-of-Sight (LOS) and NLOS patterns, enabling us to train a classifier that identifies NLOS conditions. This classifier allows us to identify which TA measurements are affected by NLOS, and thus take countermeasures to compensate the ranging error.

In summary, we make the following key contributions:

- We perform measurements in a real 5G test network deployed in a major European city, with a user carrying a 5G smartphone and moving at walking speed across different trajectories. In the experiments, the target mobile device moves as far as 461 meters of distance from the 5G base station, offering a realistic test scenario.
- We derive the analytic beam shapes, which match well with the real beams of the large antenna array. We then synthesize higher-resolution AoA measurements using the individual experimental beam shapes and their distinct properties, providing continuous signal strength measurement over the angle rather than the discrete values provided by the measured beams.
- We propose to leverage the measurements from all the communication beams of massive MIMO for identifying which AoA measurements are under NLOS with a novel Artificial Intelligence (AI) classifier of the propagation environment.
- We introduce two different methods to refine the direction (AoA) and ranging (5G TA) estimates, based on insights from the real measurements. In particular, for scenarios classified as NLOS, we separately refine the AoA and 5G TA estimation by leveraging knowledge from multiple antenna beams.

We demonstrate that our framework achieves an aggregated median positioning error of $16.5\,m$ across all experiments using measurements collected at a single commercial gNB. This represents a multifold improvement over the baseline method, consisting of using the stronger angular communication beam and the Reference Signal Received Power (RSRP) for ranging.

The rest of this paper is structured as follows. First, Sec. II refers to background information about 5G positioning and motivates our choices in the investigation. Second, Sec. III presents our real-world 5G dataset for positioning, consisting of four different trajectories with a variety of LOS and NLOS conditions over a total of 343 000 data samples. Third, Sec. IV introduces our proposed novel framework for 5G positioning and its different components to increase AoA resolution, distinguish between LOS and NLOS links, and correct multipath errors in angle and ranging measurements. Afterwards, Sec. V provides an evaluation of our proposed positioning framework in a real 5G network. Finally, related work is analyzed in Sec. VI while Sec. VII summarizes our conclusions.

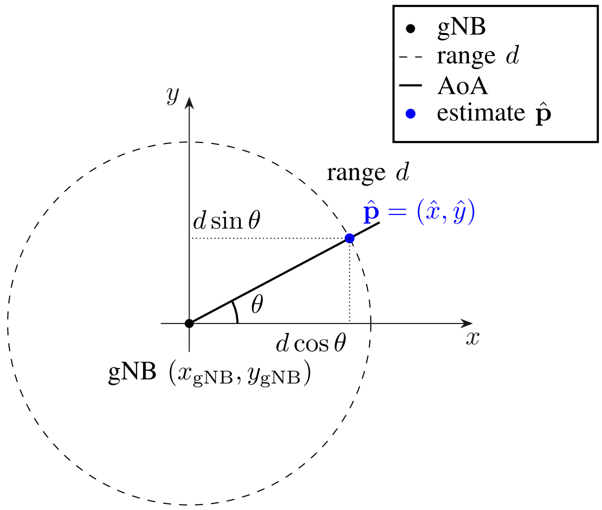

Fig. 2: NR E-CID geometry: the gNB measures the AoA θ and range d to estimate the UE position $\hat{\mathbf{p}}$ via Eq. 1.

II. Motivation and Challenges

In this section, we first review the main positioning concepts of 5G networks, motivating our choice for investigating single base-station 5G positioning, and then introduce the core challenges of this approach.

A. Motivation

The 3GPP specification has defined some key methods for positioning. These can be grouped into two categories: those requiring multiple gNBs, and those that can be performed with a single gNB. The first category includes methods based on the difference in travel time between the User Equipment (UE) and two base stations (Time Difference of Arrival, TDOA). TDOA requires network synchronization among gNBs with a precision several orders of magnitude tighter than that needed for communication. Specifically, we observe that:

- communication can typically tolerate synchronization errors on the order of microseconds [3];
- TDOA-based positioning, by contrast, demands synchronization within a few nanoseconds to achieve meter-level accuracy [4].

This gap implies significant and costly upgrades to the 5G network infrastructure.

On the contrary, NR E-CID estimates the UE's location using direction (AoA), and distance (ranging) measurements collected at a single gNB [5]. This approach eases the deployment of 5G positioning with respect to multi-gNB positioning. It could also be adopted by private network operators interested in deploying pervasive services over a given area of the city without large dedicated investments for positioning services.

NR E-CID represents a major upgrade over Enhanced Cell ID (E-CID) used in 4G networks [6] that relied on less accurate ranging (see Section II-B) and provided only sector-level AoA measurements, because most LTE eNodeBs use 2 to 4 horizontal antennas. As a result, the UE could be located only along a sector around the gNB, without the precise angular estimate needed to locate its position.

TABLE I: Resolution of 5G communication measurements for single-cell smartphone positioning.

Measurement	Resolution	Remarks
AoA	$180°/N_{\text{ant}}$ (avg)	Orthogonal beams up to N_{ant} (antenna elements)
$N_{\text{ant}} = 8$	$\approx 22.5°$	Beamwidth depends on steering angle
TA	$\Delta d = ct_{\text{TA}}/2$	Depends on subcarrier spacing
$\mu = 1$ (30 kHz)	39.06 m	Default case (this work)
$\mu = 2$ (60 kHz)	19.53 m	Higher subcarrier spacing improves resolution

Let us refer to Fig. 2. For the NR E-CID positioning method, we first estimate both the AoA, denoted as θ, and the distance between the gNB and the user, denoted as d. In order to obtain the UE's location $\hat{\mathbf{p}}$, we define a coordinate system on a two-dimensional map, where $(x_{\text{gNB}}, y_{\text{gNB}})$ denotes the position of the gNB. The estimated UE position is given by:

$$\hat{\mathbf{p}} = (\hat{x}, \hat{y}) = (x_{\text{gNB}} + d \cdot \cos\theta, y_{\text{gNB}} + d \cdot \sin\theta). \quad (1)$$

B. Challenges

The practical resolution of 5G positioning measurements depends on both angular and ranging granularity. For AoA, the resolution is limited by the number of antenna elements, which determines the beamwidth. For ranging, the resolution is set by the 5G TA measurement, which depends on the subcarrier spacing. In what follows, we describe these problems in detail, with Table I providing representative values.

AoA estimation in 5G. The beamwidth of the AoA estimate is inversely related to the array size, as a larger number of antenna elements increases the effective aperture and concentrates the radiated energy into a narrower beam. Thus, the larger set of antenna arrays in 5G MIMO allows an increase in the number of spatial beams. However, despite the improved spatial resolution, the accuracy remains limited for precise device positioning. This is because it is fundamentally constrained by the number of communication beams.

For instance, with 8 antenna elements on the horizontal plane as in the experimental array in this work, up to 8 orthogonal beams can be formed. Considering an angular coverage of 180°, this results in beamwidths on the order of tens of degrees depending on the steering angle. Therefore, new approaches are needed to enhance positioning performance, as further discussed in Section IV-A.

Ranging estimation in 5G. We discuss measurements for UE ranging that can be used by the NR E-CID method according to the 3GPP standard [5].

Reference Signal Received Power (RSRP)-based ranging: RSRP measurements can be used for distance estimation, and applied to NR E-CID positioning. However, RSRP is highly vulnerable to channel impairments, making it unreliable for UE ranging. The limitations of RSRP-based ranging are demonstrated in our evaluation section.

5G TA-based ranging: Timing Advance in 5G ensures uplink synchronization so that signals from multiple UEs arrive at the gNB simultaneously. While primarily used for communication, TA can also support NR E-CID positioning without added gNB processing.

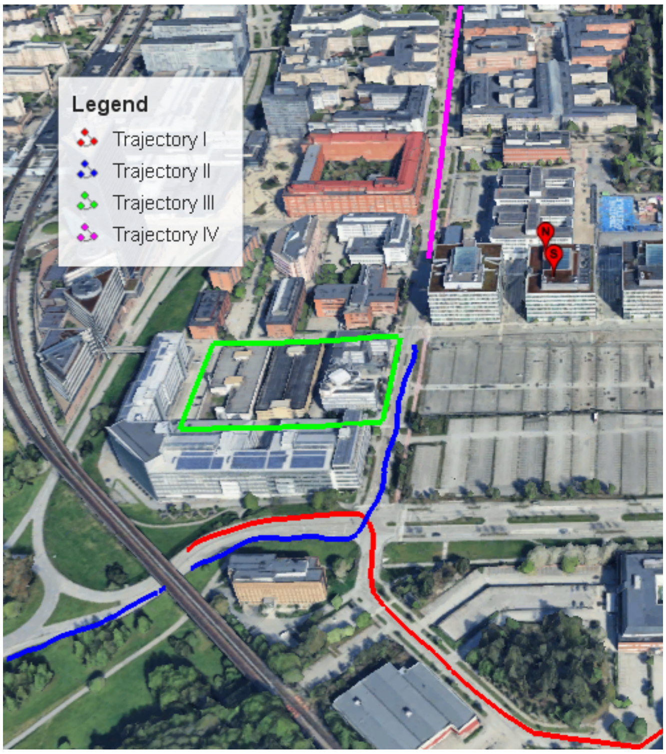

Fig. 3: Real-world experimental scenario in a major European city using commercial gNB equipment. The red markers indicate the locations of the two Transmission-Reception Points (TRPs) of the gNB in the South (S) and North (N) regions. Trajectories I, II, and III are connected to the South TRP, while Trajectory IV is connected to the North TRP.

The TA timing resolution can be derived from [7] as:

$$t_{\text{TA}} = 16 \cdot 64 \cdot \frac{T_c}{2^\mu}, \quad (2)$$

where μ is the numerology index [8], and $T_c = 0.50862\,\text{ns}$.

For a typical $\mu = 1$ as in our study (i.e., 30 kHz subcarrier spacing), this yields $t_{\text{TA}} = 260.4\,\text{ns}$. Mapping this to distance:

$$\Delta d = \frac{c \cdot t_{\text{TA}}}{2} = 39.06\,\text{m}, \quad (3)$$

where c is the speed of light and the factor 2 is for round-trip time.

The estimated distance is:

$$\hat{d} = \text{TA} \cdot \Delta d = \text{TA} \cdot \frac{c \cdot t_{\text{TA}}}{2}, \quad \text{TA} \in \mathbb{Z}_{\geq 0}. \quad (4)$$

TA resolution in 5G (39.06 m) improves over 4G (78.13 m), and can reach 19.53 m with 60 kHz subcarrier spacing. However, as discussed in Section IV-D, its accuracy degrades in NLOS conditions, motivating the need for approaches to improve its accuracy.

To investigate these challenges in practice, we next describe our real-world 5G measurement campaign. This dataset serves as the foundation for developing and evaluating our positioning framework, enabling us to quantify the limitations of current approaches and motivate the methods we propose in the following sections.

III. 5G Real-world Measurements for Positioning

A major limitation of prior work is the lack of real-world experimental study for 5G positioning. In order to address

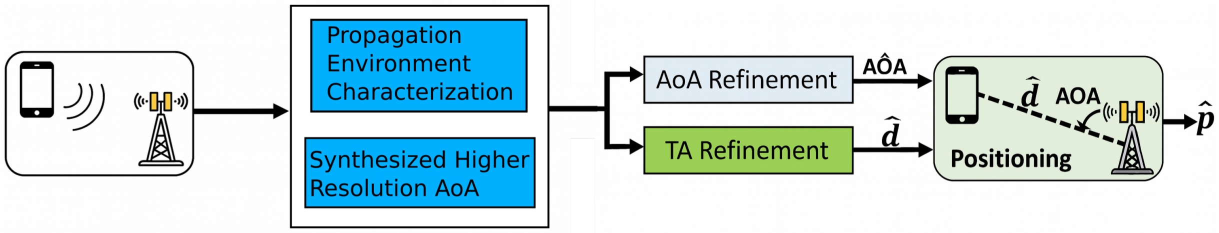

Fig. 4: Proposed 5G Positioning Framework.

this problem, we conduct measurements in a 5G test network based on 3GPP Release 15 and representative of commercial deployments. The test network is set up in the urban area of a major European city.

A. Deployment

The gNB consists of two cells, with different angular coverage for communication. The frequency of operation of the network is 3.9 GHz with 100 MHz bandwidth. Each cell uses a Transmission-Reception Point (TRP) with a planar antenna array of 8 horizontal and 4 vertical antennas for communication. Furthermore, each antenna has dual polarization. Hence, in total, each TRP consists of 64 logical antenna ports. The UE is a Sony Xperia smartphone. In the experiments, the user holding the UE walks at normal human speed.

The receiver beams at the TRP are predefined for directional communication with various UEs, and RSRP is measured at the TRP for each predefined receiver beam over the resource elements of the reference signal [9].

B. Scenarios

The scenarios depicted in Fig. 3 consist of a mix of LOS and NLOS urban environments, covering an area of approximately 0.5 km^2. The communication is considered to be LOS when there is clear visibility between the TRP and the UE without any major objects on the wireless signal path. The trajectories followed by the UE are represented by different colored lines:

- **Trajectory I:** The UE follows a path of 401 m, with minimum and maximum distances from the TRP of 244 m and 375 m, respectively.
- **Trajectory II:** The UE follows a path of 481 m, with minimum and maximum distances from the TRP of 115 m and 434 m, respectively.
- **Trajectory III:** The path length is 460 m, with minimum and maximum distances from the TRP of 112 m and 280 m, respectively.
- **Trajectory IV:** This trajectory is predominantly NLOS, with a total length of 480 m. The minimum and maximum distances between the UE and the TRP are 116 m and 461 m, respectively.

Trajectories I, II, and III are connected to the South 5G cell (red marker labeled ”S”), while Trajectory IV is connected to the North 5G cell (red marker labeled ”N”), as depicted in Fig. 3. RSRP beam values and TA are extracted at the gNB level during live network testing. The total number of data samples collected is 343 000.

Building on these real-world measurements, we now introduce our positioning framework, which leverages the collected beam and timing data to enhance angle estimation, detect NLOS conditions, and refine ranging accuracy.

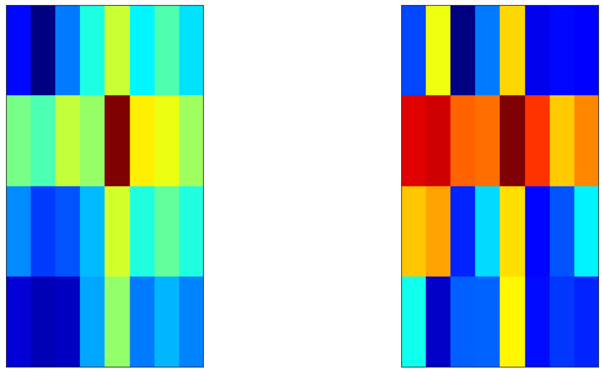

(a) LOS conditions. (b) NLOS conditions.

Fig. 5: RSRP beam pattern under different propagation environments. We show the signal strength of all the receiver beams in a grid, with 8 horizontal beams (azimuth) and 4 vertical beams (elevation).

IV. Positioning Framework

In this section, we introduce our proposed positioning framework with the procedures depicted in Fig. 4, and then present the key contributions for each step of the framework.

A. Synthesizing Higher-Resolution AoA

Although the number of receiver beams increases with the number of antenna elements in a Massive MIMO array, the resolution for AoA is still limited to a total of 8 measurements on the horizontal plane and 4 on the vertical plane as it can be observed in the RSRP measured on the horizontal and vertical planes in Fig. 5. While the resolution could be doubled by leveraging the dual antenna polarization, we find that the best results are achieved by averaging the power of both polarizations.

In principle, high-resolution AoA estimators such as MUSIC could be used to achieve super-resolution beyond the predefined beam set [10]. However, these algorithms require access to raw I/Q samples from each antenna element in order to construct the spatial covariance matrix. Such low-level signals are not available from commercial 5G gNBs, where only beamformed RSRP measurements are exposed.

To overcome this limitation, we propose to increase the AoA resolution by leveraging the knowledge of the normalized beamwidth distribution $f(\theta)$ *for each beam*, and the distribution *for different beams* in planar antenna arrays, without requiring modifications to the gNB hardware or interfaces. In the case of planar antenna arrays, the beam pattern $f_i(\theta)$ can be well approximated with a Sinc function [11], which also allows us to take into account the side lobes:

$$f_i(\theta) = \frac{\mathrm{sinc}(\theta/w_i)}{\sqrt{\int_{-\pi/2}^{\pi/2} \mathrm{sinc}^2(\theta/w_i)\, d\theta}}, \tag{5}$$

where w_i is a function of the beamwidth and the denominator indicates the total energy. The smaller w_i is, the smaller the beamwidth is. We compare the beam shapes generated through Eq. 5 with those of the commercial planar antenna arrays used in our deployment. We observe that *the proposed model accurately captures the real-world beam response*.

Second, in these commercial arrays, we observe that:

- the predefined beam directions $\{\theta_i\}$ have unequal spacing between the peak power of their azimuth angle: since beams are typically generated by sampling uniformly in spatial frequency ($u = \sin\theta$), their peak spacing in physical angle $\{\theta_{i+1} - \theta_i\}$ becomes finer in the center (0 radians) and coarser toward the edges ($\pm\ \pi/2$ radians);
- the beamwidth varies with angle: beams are narrower near the center and wider at the edges, a direct consequence of the nonlinear mapping $\Delta\theta \approx \Delta u / \cos\theta$.

For communication purposes, each beam is selected independently. However, since these beams are predefined (i.e., drawn from a fixed beam set), for positioning measurements, we experimentally observe that more than one beam can receive the signal above the sensitivity of the receiver. Therefore, for a given elevation angle, we then propose to compute the resulting total signal power $S(\theta)$ for a given θ by summing up the weighted contribution of each beam distribution.

More formally, this can be formulated as:

$$S(\theta) = \sum_{i=1}^{N_{\text{ant}}} RSRP_i \cdot f_i^2(\theta - \theta_i), \tag{6}$$

where N_{ant} indicates the total number of beams (8 in our experimental dataset) for a given elevation. The effect of this design is shown in Fig. 6 for both LOS and NLOS cases.

In summary, while the proposed beam-synthesis approach does not reach the theoretical super-resolution of MUSIC, it provides a practical, low-complexity and deployable solution for enhancing AoA estimation in commercial 5G networks, where access to raw IQ samples per antenna is restricted.

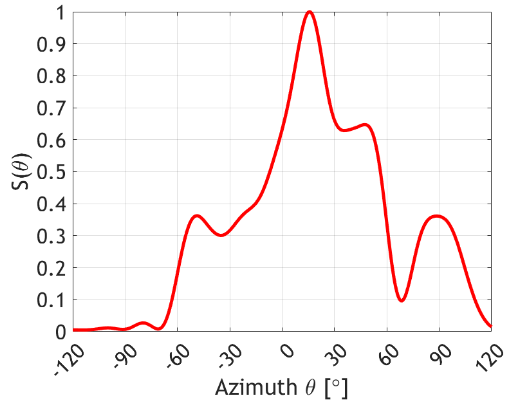

(a) LOS scenario.

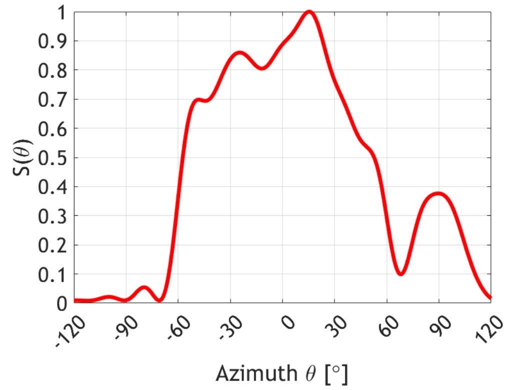

(b) NLOS scenario.

Fig. 6: AoA estimation in LOS and NLOS scenarios for a given elevation using the proposed method to synthesize higher-resolution AoA.

B. Propagation Environment Characterization

Our framework identifies the environmental complexity, that is, whether the direct path between the gNB and the smartphone is unobstructed and the strongest link, indicating a LOS measurement. We consider this step as crucial: as we will observe in our traces, there is the need to monitor the integrity of ranging measurements (5G TA) and apply environment-specific optimizations to both ranging and angle.

The messages for supporting the identification of LOS and NLOS have been introduced in the 5G specification version as part of positioning protocol [5], however the 3GPP standard does not define the algorithms for this process. To classify the LOS and NLOS conditions between a UE and a gNB, AI methods can be used, as proposed in a recent 3GPP document as part of the latest pre-6G Release 19 [12].

To achieve this, our idea is to *leverage the measurements from all the communication beams of massive MIMO for identifying which AoA measurements are under NLOS*. We then create a database of received antenna beam patterns as depicted in Fig. 5 under LOS and NLOS conditions. In the heatmap in Fig. 5, warmer colors, like red and orange, indicate stronger RSRP values. Cooler colors like blue, and yellow indicate weaker values. The intuition is that the received antenna beam pattern captures the unique propagation characteristics of the environment. This includes signal reflections and obstructions present in NLOS conditions, as well as the dominance of direct paths in LOS scenarios.

We use Convolutional Neural Networks (CNNs) for the classification task. CNNs are well suited for analyzing visual data like images. In our scenario, the heatmaps of RSRP beam patterns resemble visual data, making CNNs an appropriate choice. The network takes the antenna beam pattern heatmaps as input and is composed of a total of seven hidden layers. Two convolutional layers are applied, and each convolutional layer is followed by a 2×2 MaxPooling Layer. Then, a dropout layer is used to prevent overfitting, followed by a dense layer with 64 nodes and an output layer with 1 node for binary classification (LOS or NLOS). We mention that the ReLU activation function is used in all layers except the output layer, where a sigmoid activation function is applied to produce the final result through a probability score. We use 70% of the antenna beam patterns for training the AI model and reserve the remaining 30% for testing. To prevent overfitting, we ensure that the training and testing sets contain completely disjoint samples. The output of the AI model is an indication of whether the UE is in a LOS or NLOS location with respect to the gNB.

C. AoA Refinement

Accurate AoA estimation presents significant challenges, particularly in NLOS conditions, where signal obstructions and multipath reflections distort the AoA measurement. In such cases, selecting the AoA corresponding to the strongest peak often leads to suboptimal results. To overcome this limitation, we leverage the environmental complexity knowledge (cf. Sec. IV-B), and the higher-resolution AoA patterns (cf. Sec. IV-A) to refine the AoA estimation.

In scenarios classified as LOS, we adhere to the conventional approach by selecting the strongest peak, as it reliably corresponds to the true AoA. For instance, in the enhanced-resolution beam pattern illustrated in Fig. 6a, a LOS position is depicted where the maximum peak at 15 degrees is chosen, resulting in low AoA error.

In scenarios classified as NLOS, we adopt a different strategy by *selecting the second strongest peak, as the first is dominated by reflection*. As illustrated in Fig. 6b, the true AoA is approximately -30 degrees, yet the strongest peak appears at 15 degrees, causing a large estimation error of around 45 degrees. However, additional peaks are observed at -25, -50, and 90 degrees. By refining the AoA estimation and selecting the second strongest peak at -25 degrees, the AoA error is significantly reduced from 45 degrees to just 5 degrees.

In the case of indoor users, the relative delay/angle offsets are smaller due to confined geometry. The 3GPP standard models the dominant energy contribution as the outdoor path (LOS or a strong facade reflection), with indoor clusters heavily attenuated (see [13], Section 7.4.3). Although not experimentally verified here, this provides forward-looking insight that our AoA method remains relevant with outdoor gNB deployments and indoor users.

In summary, given the synthesized higher-resolution pattern $S(\theta)$ and the environment label, the AoA estimator is:

$$\hat{\theta} = \begin{cases} \arg\max_{\theta} S(\theta), & \text{if LOS}, \\ \text{2nd-strongest peak of } S(\theta), & \text{if NLOS}, \end{cases}$$

The statistical validity of this approach across all measurements is shown in the system evaluation in Section V.

D. 5G TA Refinement

We analyze the low accuracy of 5G TA for ranging in scenarios identified by our framework as NLOS. We focus again on Fig. 6b, which illustrates a NLOS pattern where the true distance between the TRP and the UE is $344\,m$. The 5G TA estimate is 12. From Eq. 4, this is mapped to a distance of $12 \cdot \Delta d = 468.72\,m$, leading to a significant ranging error of $\approx 124\,m$. This experiment shows that *5G TA tends to overestimate the target distance in NLOS scenarios*.

Furthermore, we note that, as previously discussed in Section IV-C, we can observe at least three peaks with $S(\theta) > 0.5$ covering an angular width from $-50°$ to $90°$, thus leading to an AoA width of $140°$. On the other hand, for the example in Fig. 6a, we observe two peaks with $S(\theta) > 0.5$ with total angular coverage of $65°$. Therefore, in the NLOS scenario, we observe that the strong AoA peaks are wider than those estimated under LOS conditions.

In order to generalize this finding, we plot in Fig. 7 the median TA error as a function of AoA width and number of peaks, respectively, for all measurements listed by our AI classifier as NLOS. Fig. 7a illustrates the increasing trend in the median TA ranging error with respect to AoA width, and in Fig. 7b we observe that a higher number of peaks correspond to greater median TA ranging errors. In particular, we often observe estimates of up to 4-5 TA units higher than the correct value, leading to an error of up to $200\,m$. Therefore, this study confirms that in NLOS scenarios, AoA distributions with high peaks are wider than expected in the presence of a single dominant peak.

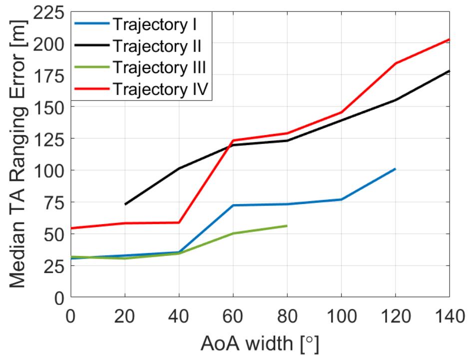

(a) Median TA error and AoA width among peaks.

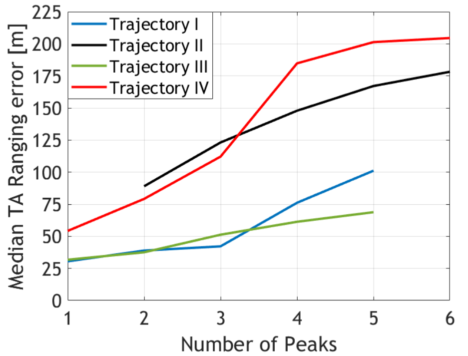

(b) Median TA error and number of peaks.

Fig. 7: TA overestimation problem and its relation to AoA width and number of peaks under NLOS conditions.

We note that, while the exact number of peaks depends on deployment, the trend (wider AoA spread and higher peak count in NLOS versus LOS) is consistent with propagation theory and has been observed across all four trajectories in our study. We then propose an *empirically-driven adjustment to the 5G TA estimate* to mitigate the impact of the large number of peaks and wide AoA distribution in NLOS links:

$$\mathrm{TA}_{\mathrm{adj}} = \mathrm{TA} - N_{\mathrm{peaks}} \cdot \left(\frac{w_{\mathrm{AoA}}}{\pi}\right) \tag{7}$$

where:

- $\mathrm{TA}_{\mathrm{adj}}$ is the adjusted timing advance;
- N_{peaks} is the number of significant AoA peaks, with $S(\theta) > 0.5$;
- w_{AoA} is the total angular spread (in radians) of the AoA distribution with $S(\theta) > 0.5$.

We note that while TA is an integer, $\mathrm{TA}_{\mathrm{adj}}$ is a real number.

E. Positioning

We compute the position estimate using the angle and range estimators described in the previous sections. In this study, we assume that the UE is located at ground level, while

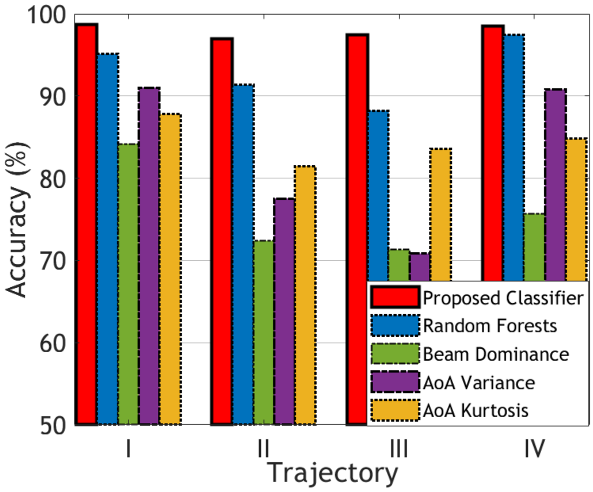

Fig. 8: Accuracy of the proposed CNN-based classifier for distinguishing between LOS and NLOS conditions using 5G RSRP measurements, outperforming alternative methods.

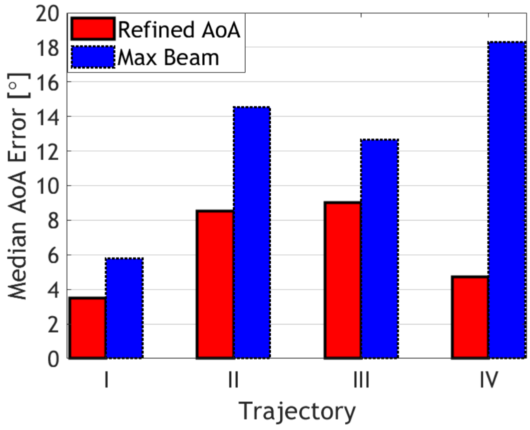

Fig. 9: Median AoA error for our proposed estimator (red bar) compared to the alternative (blue bar).

the gNB is positioned at a given altitude. The estimated distance is then projected onto the 2D plane, and the location is inferred according to Eq. 1. The extension to 3D positioning requires leveraging the knowledge from the elevation plane, similarly to the approach presented for the azimuth plane in Section IV-A.

In order to improve the position accuracy, state-space filters (e.g., Kalman filtering) could be applied. However, they are more effective when fusing heterogeneous measurements (e.g., with inertial sensors as in GNSS) or when a well-defined motion model is available (e.g. the movement is constrained to a road). Furthermore, for pedestrian kinematics, the displacement over tens of milliseconds is much smaller than TA resolution and comparable to AoA granularity, thus a state-space filter may have mis-tuning problems.

In turn, as our scenario relies solely on single-cell measurements of AoA and TA, a lightweight temporal smoothing mechanism is more appropriate. Therefore, we smooth the location estimate with an Exponentially Weighted Moving Average (EWMA) filter:

$$\bar{\mathbf{p}}_{\mathbf{k}} = (1-\alpha)\bar{\mathbf{p}}_{\mathbf{k-1}} + \alpha\hat{\mathbf{p}}_{\mathbf{k}}, \quad s.t. \quad \bar{\mathbf{p}}_{\mathbf{1}} = \hat{\mathbf{p}}_{\mathbf{1}} \tag{8}$$

where $\hat{\mathbf{p}}_{\mathbf{k}}$ is the current position estimated as in Eq. 1, $\bar{\mathbf{p}}_{\mathbf{k-1}}$ is the previous smoothed position estimate and α is the filter weight. α puts more or less weight on historical values according to its value. In our system, we leverage the knowledge of the propagation environment characteristics with our LOS and NLOS classifier presented in Section IV-B, and we give more weight to a measurement $\hat{\mathbf{p}}_{\mathbf{k}}$ classified as LOS ($\alpha = \alpha_{LOS}$), and less weight if it is classified as NLOS ($\alpha = \alpha_{NLOS}$).

V. System evaluation

In this section, we first evaluate the accuracy of our proposed LOS/NLOS classifier for environmental complexity characterization. We then discuss the accuracy of our proposed AoA and ranging methods. Finally, we fuse the different methods to evaluate the positioning accuracy of our framework.

A. Environmental Complexity

We compare our CNN-based classifier (cf. Section IV-B) with alternative Machine Learning and statistical methods:

Random Forests: A Random Forest classifier that uses the RSRP beam pattern as input and consists of a total of 200 decision trees with maximum depth equal to 5.

Beam Dominance: This method assesses beam dominance by computing the ratio of the strongest RSRP to the sum of all beams. A high ratio suggests a dominant LOS beam.

Angular variance: This method computes the AoA variance of dominant RSRP beams, which is typically low under LOS due to concentrated angular energy.

Angular kurtosis: This method calculates the AoA kurtosis corresponding to significant RSRP beams. High angular kurtosis indicates a concentrated angular distribution (LOS).

Google Earth Pro is used to inspect and visualize the environment around the gNB and the UE [14], providing the ground truth for LOS and NLOS conditions through visible obstructions along the signal path. The results in Fig. 8 show that our proposed classifier provides the best performance.

B. AoA

In this section, we evaluate the accuracy of our refined AoA estimator, based on the contributions in Sec. IV-A, IV-B, and IV-C. The map of the four trajectories under study is used to compute the ground truth AoA for the evaluation. To demonstrate the effectiveness of our approach, we compare it to a baseline method that always selects the AoA corresponding to the strongest beam, the "Max Beam" method.

First, Fig. 9 presents the median error of the AoA estimation, measured in degrees, for both algorithms across all trajectories. As observed, our estimator consistently achieves the lowest AoA error, improving accuracy by approximately 40%, 42%, 29%, and 75% compared to the baseline method across the four trajectories, respectively.

C. Ranging

We evaluate the ranging performance of our refined TA estimator, based on the contributions in Sec. IV-B and IV-D. Fig. 10 shows the median ranging error in meters for all trajectories. We first analyze the performance of our proposed ranging estimator (green bars) in NLOS positions and compare it with the results of the non-refined TA (blue bars) in the same set of NLOS measurements. Our estimator yields

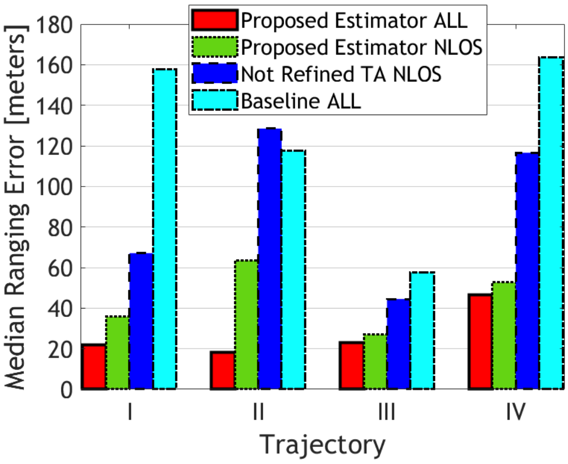

Fig. 10: Median ranging error for our proposed estimator (red and green bars) compared to alternatives.

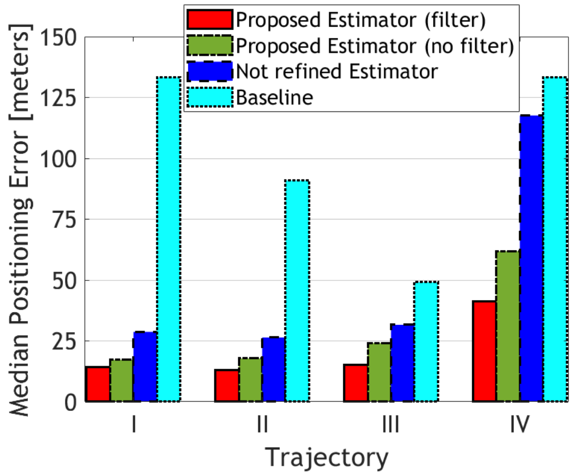

Fig. 11: Median positioning error for our proposed estimator and alternatives.

improvements of approximately 47%, 51%, 40%, and 55% compared to the non-refined TA method across the four trajectories, respectively, thereby validating the effectiveness of Eq. 7.

The figure also shows a baseline estimator (cyan bars). The baseline applies a path-loss model for ranging based on the beam with the highest RSRP, assigning different path-loss exponents for LOS and NLOS positions to reflect their propagation differences. Finally, the red bars illustrate the performance of our estimator across both LOS and NLOS positions. The results in Fig. 10 demonstrate that our proposed estimator significantly outperforms the baseline method, achieving a ranging gain of $\approx$ 79%.

Our proposed estimator is the most effective ranging solution, consistently outperforming all alternatives in both LOS and NLOS scenarios.

D. Positioning

In this section, we study the positioning error. Our estimator applies an EWMA filter with $\alpha_{NLOS} = 0.03$ for a measurement classified by our algorithm as a NLOS link, and $\alpha_{LOS} = 0.1$ for a measurement classified as LOS (see Sec. IV-E). In this way, it provides more weight to measurements that are more reliable. Other values could also be chosen based on the desired trade-off between the frequency of NLOS conditions and the balance between UE tracking and positioning accuracy.

We compare our proposed positioning estimator (red bars) against alternative methods. First, we evaluate the performance of an estimator (green bars) that does not utilize the EWMA filter introduced in Sec. IV-E. In addition, we consider a non-refined estimator that selects the maximum communication beam for AoA estimate in the 8×4 antenna array and uses the non-refined TA value for ranging (blue bars). Finally, we include a baseline approach that uses the maximum beam for AoA estimate and the RSRP for ranging (cyan bars). After obtaining the AoA and ranging estimates, the UE position is estimated as explained in Sec. II-A.

We summarize the results in Fig. 11, which presents the median positioning error in meters obtained by our estimator compared with the other approaches across all trajectories. The results indicate that our estimator consistently outperforms all alternatives, yielding lower positioning error across every trajectory. Specifically, the average gain in positioning error is approximately 45%, 27%, 42% and 29% with respect to the non-filtered estimator; 59%, 55%, 57% and 59% with respect to the non-refined estimator; and 86%, 73%, 65% and 64% with respect to the baseline across the four different trajectories, respectively.

When considering all four trajectories, our estimator achieves an aggregated median positioning error of $16.5\,m$, demonstrating a substantial improvement over alternative methods that exhibit median aggregated positioning errors of $27.6\,m$, $40.5\,m$ and $86.8\,m$ (the latter being the baseline).

VI. Related Work

To the best of our knowledge, we are the first to investigate user positioning with a single commercial gNB and an off-the-shelf smartphone using a 5G-compliant positioning method.

Single gNB positioning systems: Experimental research on single gNB positioning is limited, primarily due to the high cost and hardware constraints of Software-Defined Radio (SDR) platforms, which often lack the antenna arrays required for practical AoA-based measurements. They provide only a few antenna outputs (e.g., 2 antennas in [15]) compared to commercial gNBs designed to support MIMO. Existing studies often rely on lab-based SDR environments [15], [16] or only simulation results [17], [18], [19], frequently requiring specialized reference signals unavailable in commercial deployments. Recent 5G NR works utilize commercial 5G networks [20], [21], [22], [23] or SDR testbeds [24], [25], [26], but they use USRPs as UEs for downlink measurements, which are inaccessible on standard smartphones. Furthermore, other methods either provide limited context like floor-level inference [27] or require access to restricted channel data [28]. In contrast, our framework is evaluated in a real-world 5G test network with a commercial massive-MIMO gNB and an off-the-shelf smartphone, relying only on 5G communication measurements rather than specialized UE hardware or raw per-antenna I/Q samples.

Other positioning systems: A few papers have considered more than one gNB. For instance, [29] studied a multi-gNB positioning system in 5G, requiring access to physical signals to estimate the synchronization error between the gNBs, a limitation that our estimator does not have. [4] utilizes the Positioning Reference Signal (PRS) on the downlink, but requires a non-commodity UE that measures the TDOA of the PRS obtained by multiple gNBs. In contrast, our framework can be applied to commodity smartphones. Our method uses only uplink measurements required for communication, which are produced independently of network load. Therefore, unlike multi-gNB positioning based on positioning signals, it does not degrade under multi-user traffic. Finally, many works utilize AI fingerprinting approaches in SDR testbeds [30], [31], [32], but have not been tested under real 5G NR commercial scenarios as our proposed system.

VII. Conclusion

We performed the first study of 5G single-cell communication signals applied to pervasive smartphone positioning. We collected measurements from a 5G test network deployed in a major European city, using a commercial gNB with massive MIMO as the base station and a consumer smartphone as the UE. The study has shown that simple estimators based on the strongest communication beam and uncorrected Timing Advance provide poor positioning accuracy. We have introduced methods to increase the resolution of Angle of Arrival measurements leveraging the individual beam shapes of realistic massive MIMO 5G antenna arrays, a novel CNN-based classifier of LOS and NLOS conditions, and empirically-driven methods to correct the errors of angle and distance measurements. Our proposed framework can be easily integrated in future 5G deployments as it relies only on communication measurements, without requiring specialized UE hardware, raw per-antenna I/Q samples, tight inter-gNB synchronization, or external sensors. This capability is particularly relevant to pervasive computing scenarios, easing deployment for public and private network operators.

Acknowledgement

The work at IMDEA Networks was supported by 6G-ELSA project PID2022-136769NB-I00 funded by MCIN/ AEI /10.13039/501100011033/.

The authors thank Nicklas Johansson for his valuable support throughout this work.

References

[1] K. Merry and P. Bettinger, "Smartphone GPS accuracy study in an urban environment," *PloS one*, vol. 14, no. 7, p. e0219890, 2019.

[2] "3GPP TS 38.305, NG Radio Access Network (NG-RAN); Stage 2 functional specification of User Equipment (UE) positioning in NG-RAN, Rel. 19," 3rd Generation Partnership Project (3GPP), 2026.

[3] 3rd Generation Partnership Project (3GPP), "TS 38.133: NR; Requirements for support of radio resource management," 3GPP, Tech. Rep., 2025, clause 7.4.2, Cell phase synchronization accuracy.

[4] I. Palamà, Y. Lizarribar, L. M. Monteforte, G. Santaromita, S. Bartoletti, D. Giustiniano, G. Bianchi, and N. B. Melazzi, "5G positioning with software-defined radios," *Computer Networks*, p. 110595, 2024.

[5] "3GPP TS 38.455, NG-RAN; NR Positioning Protocol A (NRPPa), Rel. 18," 3rd Generation Partnership Project (3GPP), 2025.

[6] "3GPP TS 36.305, Evolved Universal Terrestrial Radio Access Network (E-UTRAN); Stage 2 functional specification of User Equipment (UE) positioning in E-UTRAN, Rel. 18," 3rd Generation Partnership Project (3GPP), 2025.

[7] "3GPP TS 38.211, Physical channels and modulation, Rel. 18," 3rd Generation Partnership Project (3GPP), 2025.

[8] "3GPP TS 38.213, NR; Physical layer procedures for control, Rel. 18," 3rd Generation Partnership Project (3GPP), 2025.

[9] "3GPP TS 38.215, NR; Physical layer measurements," 3rd Generation Partnership Project (3GPP), 2025.

[10] R. Schmidt, "Multiple emitter location and signal parameter estimation," *IEEE transactions on antennas and propagation*, vol. 34, no. 3, pp. 276–280, 1986.

[11] W. Guo, W. Zhang, P. Mu, F. Gao, and H. Lin, "High-Mobility Wideband Massive MIMO Communications: Doppler Compensation, Analysis, and Scaling Laws," *IEEE Transactions on Wireless Communications*, vol. 18, no. 6, pp. 3177–3191, 2019. [Online]. Available: https://arxiv.org/pdf/1807.07438

[12] "3GPP TR 38.843, Study on Artificial Intelligence (AI)/Machine Learning (ML) for NR air interface, Rel. 19," 3rd Generation Partnership Project (3GPP), 2025.

[13] "3GPP TR 38.901, Study on channel model for frequencies from 0.5 to 100 GHz, Rel. 19," 3rd Generation Partnership Project (3GPP), 2026.

[14] Google, "Google Earth Pro," 2025, accessed: 2026-04. [Online]. Available: https://www.google.com/earth/versions/earth-pro

[15] D. Li, X. Chu, L. Wang, Z. Lu, S. Zhou, and X. Wen, "Performance Evaluation of E-CID based Positioning on OAI 5G-NR Testbed," in *2022 IEEE/CIC International Conference on Communications in China (ICCC)*, 2022, pp. 832–837.

[16] A. Blanco, N. Ludant, P. J. Mateo, Z. Shi, Y. Wang, and J. Widmer, "Performance evaluation of single base station ToA-AoA localization in an LTE testbed," in *2019 IEEE 30th annual international symposium on personal, Indoor and Mobile Radio Communications (PIMRC)*. IEEE, 2019, pp. 1–6.

[17] B. Sun, B. Tan, W. Wang, and E. S. Lohan, "A comparative study of 3D UE positioning in 5G new radio with a single station," *Sensors*, vol. 21, no. 4, p. 1178, 2021.

[18] B. Sun, B. Tan, W. Wang, M. Valkama, C. Morlaas, and E.-S. Lohan, "5g positioning based on the wideband electromagnetic vector antenna," in *WiP Proceedings of the International Conference on Localization and GNSS (ICL-GNSS 2021)*. CEUR-WS, 2021.

[19] Y. Wang, Q. Wu, M. Zhou, X. Yang, W. Nie, and L. Xie, "Single base station positioning based on multipath parameter clustering in NLOS environment," *EURASIP Journal on Advances in Signal Processing*, vol. 2021, no. 1, p. 20, 2021.

[20] W. Dong, L. Chen, Z. Ju, Z. Jiao, and R. Chen, "Time-of-Arrival Estimation in Challenging Environments Using Commercial 5G NR Signals for Outdoor Positioning," *IEEE Internet of Things Journal*, 2025.

[21] X. Zhou, L. Chen, Y. Ruan, T. Zhou, and R. Chen, "IMPos: Indoor Mobile Positioning with 5G Multi-Beam Signals from a Single-Base-Station," *IEEE Internet of Things Journal*, 2024.

[22] Y. Ruan, L. Chen, X. Zhou, G. Guo, and R. Chen, "Hi-Loc: Hybrid indoor localization via enhanced 5G NR CSI," *IEEE Transactions on Instrumentation and Measurement*, vol. 71, pp. 1–15, 2022.

[23] Y. Ruan, L. Chen, X. Zhou, Z. Liu, X. Liu, G. Guo, and R. Chen, "iPos-5G: Indoor positioning via commercial 5G NR CSI," *IEEE Internet of Things Journal*, vol. 10, no. 10, pp. 8718–8733, 2022.

[24] X. Zhou, L. Chen, Y. Ruan, and R. Chen, "Indoor localization with multi-beam of 5G new radio signals," *IEEE Transactions on Wireless Communications*, 2024.

[25] R. Mundlamuri, R. Gangula, F. Kaltenberger, and R. Knopp, "Novel round trip time estimation in 5G NR," *arXiv preprint*, 2024.

[26] T. Spanos, F. Fabra, J. A. López-Salcedo, G. Seco-Granados, N. Kanistras, I. Lapin, and V. Paliouras, "USRP-Based Single Anchor Positioning: AoA with 5G Uplink Signals, and UWB Ranging," in *2024 11th Workshop on Satellite Navigation Technology (NAVITEC)*. IEEE, 2024.

[27] S. Mostafa, K. A. Harras, and M. Youssef, "UniCellular: An accurate and ubiquitous floor identification system using single cell tower information," in *Proceedings of the 31st ACM International Conference on Advances in Geographic Information Systems*, 2023, pp. 1–10.

[28] S. Eleftherakis, G. Santaromita, M. Rea, X. Costa-Pérez, and D. Giustiniano, "SPRING+: Smartphone Positioning from a Single WiFi Access Point," *IEEE Transactions on Mobile Computing*, 2024.

[29] B. Camajori Tedeschini, M. Brambilla, L. Italiano, S. Reggiani, D. Vaccarono, M. Alghisi, L. Benvenuto, A. Goia, E. Realini, F. Grec *et al.*, "A feasibility study of 5G positioning with current cellular network deployment," *Scientific reports*, vol. 13, no. 1, p. 15281, 2023.

[30] M. Gucciardo, I. Tinnirello, G. M. Dell'Aera, and M. Caretti, "A flexible 4G/5G control platform for fingerprint-based indoor localization," in *IEEE INFOCOM 2019-IEEE conference on computer communications workshops (INFOCOM WKSHPS)*. IEEE, 2019, pp. 744–749.

[31] W. Li, X. Meng, Z. Zhao, Z. Liu, C. Chen, and H. Wang, "LoT: A Transformer-Based Approach Based on Channel State Information for Indoor Localization," *IEEE Sensors Journal*, vol. 23, no. 22, pp. 28 205–28 219, 2023.

[32] S. Horsmanheimo, S. Lembo, L. Tuomimaki, S. Huilla, P. Honkamaa, M. Laukkanen, and P. Kemppi, "Indoor positioning platform to support 5G location based services," in *2019 IEEE International Conference on Communications Workshops (ICC Workshops)*. IEEE, 2019, pp. 1–6.